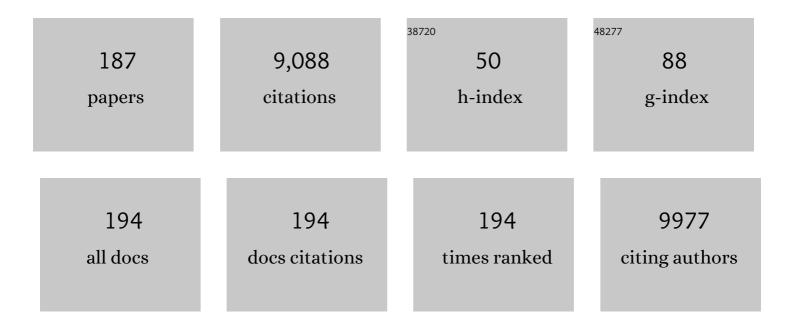
## Tsunehiro Tanaka

List of Publications by Year in descending order

Source: https://exaly.com/author-pdf/3052080/publications.pdf Version: 2024-02-01



#	Article	IF	CITATIONS
1	Thermally stable single atom Pt/m-Al2O3 for selective hydrogenation and CO oxidation. Nature Communications, 2017, 8, 16100.	5.8	545
2	Ultrathin rhodium nanosheets. Nature Communications, 2014, 5, 3093.	5.8	428
3	A Series of NiM (M = Ru, Rh, and Pd) Bimetallic Catalysts for Effective Lignin Hydrogenolysis in Water. ACS Catalysis, 2014, 4, 1574-1583.	5.5	421
4	Photocatalytic Conversion of CO <sub>2</sub> in Water over Layered Double Hydroxides. Angewandte Chemie - International Edition, 2012, 51, 8008-8011.	7.2	291
5	Selective Amine Oxidation Using Nb <sub>2</sub> O <sub>5</sub> Photocatalyst and O <sub>2</sub> . ACS Catalysis, 2011, 1, 1150-1153.	5.5	258
6	X-ray absorption (EXAFS/XANES) study of supported vanadium oxide catalysts. Structure of surface vanadium oxide species on silica and γ-alumina at a low level of vanadium loading. Journal of the Chemical Society Faraday Transactions I, 1988, 84, 2987.	1.0	238
7	Photocatalytic Reduction of CO2to CO in the Presence of H2or CH4as a Reductant over MgO. Journal of Physical Chemistry B, 2004, 108, 346-354.	1.2	237
8	Adsorbed Species of CO <sub>2</sub> and H <sub>2</sub> on Ga <sub>2</sub> O <sub>3</sub> for the Photocatalytic Reduction of CO <sub>2</sub> . Journal of Physical Chemistry C, 2010, 114, 8892-8898.	1.5	181
9	In situ spectroscopy-guided engineering of rhodium single-atom catalysts for CO oxidation. Nature Communications, 2019, 10, 1330.	5.8	177
10	Zeoliteâ€Encaged Pd–Mn Nanocatalysts for CO <sub>2</sub> Hydrogenation and Formic Acid Dehydrogenation. Angewandte Chemie - International Edition, 2020, 59, 20183-20191.	7.2	175
11	Catalytic amino acid production from biomass-derived intermediates. Proceedings of the National Academy of Sciences of the United States of America, 2018, 115, 5093-5098.	3.3	168
12	XAFS Study of Tungsten L <sub>1</sub> - and L <sub>3</sub> -Edges:  Structural Analysis of WO <sub>3</sub> Species Loaded on TiO <sub>2</sub> as a Catalyst for Photo-oxidation of NH <sub>3</sub> . Journal of Physical Chemistry C, 2008, 112, 6869-6879.	1.5	161
13	Effect of Ti <sup>3+</sup> Ions and Conduction Band Electrons on Photocatalytic and Photoelectrochemical Activity of Rutile Titania for Water Oxidation. Journal of Physical Chemistry C, 2016, 120, 6467-6474.	1.5	147
14	Photocatalytic reduction of CO2 using H2 as reductant over ATaO3 photocatalysts (A = Li, Na, K). Applied Catalysis B: Environmental, 2010, 96, 565-568.	10.8	135
15	Photocatalytic conversion of CO2 in water over Ag-modified La2Ti2O7. Applied Catalysis B: Environmental, 2015, 163, 241-247.	10.8	133
16	Deconvolution Analysis of Ga K-Edge XANES for Quantification of Gallium Coordinations in Oxide Environments. Journal of Physical Chemistry B, 1998, 102, 10190-10195.	1.2	128
17	A Doping Technique that Suppresses Undesirable H <sub>2</sub> Evolution Derived from Overall Water Splitting in the Highly Selective Photocatalytic Conversion of CO <sub>2</sub> in and by Water. Chemistry - A European Journal, 2014, 20, 9906-9909.	1.7	119
18	Photoreduction of CO2 with H2 over ZrO2. A study on interaction of hydrogen with photoexcited CO2. Physical Chemistry Chemical Physics, 2000, 2, 2635-2639.	1.3	117

#	Article	IF	CITATIONS
19	Metalâ€Dependent Support Effects of Oxyhydrideâ€Supported Ru, Fe, Co Catalysts for Ammonia Synthesis. Advanced Energy Materials, 2018, 8, 1801772.	10.2	111
20	Effect of H2 gas as a reductant on photoreduction of CO2 over a Ga2O3 photocatalyst. Chemical Physics Letters, 2008, 467, 191-194.	1.2	109
21	Highly efficient photocatalytic conversion of CO <sub>2</sub> into solid CO using H <sub>2</sub> O as a reductant over Ag-modified ZnGa <sub>2</sub> O <sub>4</sub> . Journal of Materials Chemistry A, 2015, 3, 11313-11319.	5.2	103
22	Analysis of XANES for identification of highly dispersed transition metal oxides on supports. Catalysis Letters, 1992, 12, 277-285.	1.4	102
23	Mechanism of Photooxidation of Alcohol over Nb <sub>2</sub> O <sub>5</sub> . Journal of Physical Chemistry C, 2009, 113, 18713-18718.	1.5	102
24	Photoreduction of carbon dioxide by hydrogen over magnesium oxide. Physical Chemistry Chemical Physics, 2001, 3, 1108-1113.	1.3	101
25	Reaction mechanism in the photoreduction of CO2 with CH4 over ZrO2. Physical Chemistry Chemical Physics, 2000, 2, 5302-5307.	1.3	97
26	Tuning the selectivity toward CO evolution in the photocatalytic conversion of CO <sub>2</sub> with H <sub>2</sub> O through the modification of Ag-loaded Ga <sub>2</sub> O <sub>3</sub> with a ZnGa <sub>2</sub> O <sub>4</sub> layer. Catalysis Science and Technology, 2016, 6, 1025-1032.	2.1	94
27	Supported Tantalum Oxide Catalysts:Â Synthesis, Physical Characterization, and Methanol Oxidation Chemical Probe Reaction. Journal of Physical Chemistry B, 2003, 107, 5243-5250.	1.2	93
28	Modification of Metal Nanoparticles with TiO <sub>2</sub> and Metalâ^'Support Interaction in Photodeposition. ACS Catalysis, 2011, 1, 187-192.	5.5	88
29	Highly selective photocatalytic conversion of CO2 by water over Ag-loaded SrNb2O6 nanorods. Applied Catalysis B: Environmental, 2017, 218, 770-778.	10.8	86
30	Study on the Dispersion of Nickel Ions in the NiOâ^'MgO System by X-ray Absorption Fine Structure. The Journal of Physical Chemistry, 1996, 100, 2302-2309.	2.9	85
31	Elucidating strong metal-support interactions in Pt–Sn/SiO2 catalyst and its consequences for dehydrogenation of lower alkanes. Journal of Catalysis, 2018, 365, 277-291.	3.1	84
32	Identification and reactivity of a surface intermediate in the photoreduction of CO2 with H2 over ZrO2. Journal of the Chemical Society, Faraday Transactions, 1998, 94, 1875-1880.	1.7	81
33	One-electron reducibility of isolated copper oxide on alumina for selective NO–CO reaction. Applied Catalysis B: Environmental, 2006, 64, 282-289.	10.8	77
34	Effect of the chloride ion as a hole scavenger on the photocatalytic conversion of CO <sub>2</sub> in an aqueous solution over Ni–Al layered double hydroxides. Physical Chemistry Chemical Physics, 2015, 17, 17995-18003.	1.3	76
35	A Theoretical Investigation on CO Oxidation by Singleâ€Atom Catalysts M <sub>1</sub> /γâ€Al <sub>2</sub> O <sub>3</sub> (M=Pd, Fe, Co, and Ni). ChemCatChem, 2017, 9, 1222-122	9 <mark>.<sup>1.8</sup></mark>	76
36	Structures and Acidâ~'Base Properties of La/Al2O3 Role of La Addition to Enhance Thermal Stability of γ-Al2O3. Chemistry of Materials, 2003, 15, 4830-4840.	3.2	74

#	Article	IF	CITATIONS
37	NO reduction with CO in the presence of O2 over Al2O3-supported and Cu-based catalysts. Physical Chemistry Chemical Physics, 2002, 4, 2449-2458.	1.3	72
38	Structures of Molybdenum Species in Silica-Supported Molybdenum Oxide and Alkali-Ion-Modified Silica-Supported Molybdenum Oxide. Journal of Physical Chemistry B, 1998, 102, 2960-2969.	1.2	65
39	Liquid phase photooxidation of alcohol over niobium oxide without solvents. Catalysis Today, 2007, 120, 233-239.	2.2	65
40	Preparation of Active Absorbent for Dry-Type Flue Gas Desulfurization from Calcium Oxide, Coal Fly Ash, and Gypsum. Industrial & Engineering Chemistry Research, 2000, 39, 1390-1396.	1.8	62
41	Strong metal-support interaction between Pt and SiO <sub>2</sub> following high-temperature reduction: a catalytic interface for propane dehydrogenation. Chemical Communications, 2017, 53, 6937-6940.	2.2	61
42	Reaction Mechanism of Selective Photooxidation of Amines over Niobium Oxide: Visible-Light-Induced Electron Transfer between Adsorbed Amine and Nb2O5. Journal of Physical Chemistry C, 2013, 117, 442-450.	1.5	59
43	Rutile titanium dioxide prepared by hydrogen reduction of Degussa P25 for highly efficient photocatalytic hydrogen evolution. Catalysis Science and Technology, 2016, 6, 5693-5699.	2.1	58
44	XAFS study of zirconia-supported copper catalysts for the NO–CO reaction: Deactivation, rejuvenation and stabilization of Cu species. Journal of the Chemical Society, Faraday Transactions, 1998, 94, 3743-3752.	1.7	57
45	Photocatalytic Conversion of CO2 by H2O over Ag-Loaded SrO-Modified Ta2O5. Bulletin of the Chemical Society of Japan, 2015, 88, 431-437.	2.0	56
46	Effective Driving of Ag-Loaded and Al-Doped SrTiO <sub>3</sub> under Irradiation at λ > 300 nm for the Photocatalytic Conversion of CO <sub>2</sub> by H <sub>2</sub> O. ACS Applied Energy Materials, 2020, 3, 1468-1475.	2.5	56
47	Dynamic Behavior of Rh Species in Rh/Al <sub>2</sub> O <sub>3</sub> Model Catalyst during Three-Way Catalytic Reaction: An <i>Operando</i> X-ray Absorption Spectroscopy Study. Journal of the American Chemical Society, 2018, 140, 176-184.	6.6	55
48	Which is an Intermediate Species for Photocatalytic Conversion of CO <sub>2</sub> by H <sub>2</sub> O as the Electron Donor: CO <sub>2</sub> Molecule, Carbonic Acid, Bicarbonate, or Carbonate Ions?. Journal of Physical Chemistry C, 2017, 121, 8711-8721.	1.5	54
49	Modification of Ga <sub>2</sub> O <sub>3</sub> by an Ag–Cr core–shell cocatalyst enhances photocatalytic CO evolution for the conversion of CO <sub>2</sub> by H <sub>2</sub> O. Chemical Communications, 2018, 54, 1053-1056.	2.2	53
50	Effect of reduction method on the activity of Pt–Sn/SiO2 for dehydrogenation of propane. Catalysis Today, 2014, 232, 33-39.	2.2	52
51	Structure of Active Species in Alkali-Ion-Modified Silica-Supported Vanadium Oxide. Journal of Physical Chemistry B, 1997, 101, 9035-9040.	1.2	50
52	Dehydrogenation of Propane over Silicaâ€Supported Platinum–Tin Catalysts Prepared by Direct Reduction: Effects of Tin/Platinum Ratio and Reduction Temperature. ChemCatChem, 2014, 6, 2680-2691.	1.8	49
53	Visible Light Absorbed NH <sub>2</sub> Species Derived from NH <sub>3</sub> Adsorbed on TiO <sub>2</sub> for Photoassisted Selective Catalytic Reduction. Journal of Physical Chemistry C, 2007, 111, 14189-14197.	1.5	48
54	Popping of Graphite Oxide: Application in Preparing Metal Nanoparticle Catalysts. Advanced Materials, 2015, 27, 4688-4694.	11.1	48

#	Article	IF	CITATIONS
55	Reaction Mechanism of Selective Photooxidation of Hydrocarbons over Nb <sub>2</sub> O <sub>5</sub> . Journal of Physical Chemistry C, 2011, 115, 19320-19327.	1.5	46
56	A ZnTa <sub>2</sub> O <sub>6</sub> photocatalyst synthesized via solid state reaction for conversion of CO <sub>2</sub> into CO in water. Catalysis Science and Technology, 2016, 6, 4978-4985.	2.1	46
57	Alumina-Supported Rare-Earth Oxides Characterized by Acid-Catalyzed Reactions and Spectroscopic Methods. Journal of Physical Chemistry B, 2001, 105, 1908-1916.	1.2	45
58	Effects of reaction temperature on the photocatalytic activity of photo-SCR of NO with NH3 over a TiO2 photocatalyst. Catalysis Science and Technology, 2013, 3, 1771.	2.1	45
59	Local Structure and La L <sub>1</sub> and L <sub>3</sub> -Edge XANES Spectra of Lanthanum Complex Oxides. Inorganic Chemistry, 2014, 53, 6048-6053.	1.9	44
60	Structure of Moâ^'Mg Binary Oxides in Oxidized/Reduced States Studied by X-ray Absorption Spectroscopy at the Mo K Edge and Mg K Edge. The Journal of Physical Chemistry, 1996, 100, 5440-5446.	2.9	43
61	Photocatalytic conversion of CO2 in an aqueous solution using various kinds of layered double hydroxides. Catalysis Today, 2015, 251, 140-144.	2.2	43
62	Oxygen storage capacity of Sr <sub>3</sub> Fe <sub>2</sub> O <sub>7â^î^</sub> having high structural stability. Journal of Materials Chemistry A, 2015, 3, 13540-13545.	5.2	43
63	Enhancement of CO Evolution by Modification of Ga <sub>2</sub> O <sub>3</sub> with Rare-Earth Elements for the Photocatalytic Conversion of CO <sub>2</sub> by H <sub>2</sub> O. Langmuir, 2017, 33, 13929-13935.	1.6	43
64	A nanoLDH catalyst with high CO <sub>2</sub> adsorption capability for photo-catalytic reduction. Journal of Materials Chemistry A, 2018, 6, 9684-9690.	5.2	43
65	Physico-chemical and catalytic properties of ytterbium introduced into Y-zeolite. Journal of the Chemical Society, Faraday Transactions, 1993, 89, 3177.	1.7	41
66	Deactivation Mechanism of Pd/CeO <sub>2</sub> –ZrO <sub>2</sub> Three-Way Catalysts Analyzed by Chassis-Dynamometer Tests and <i>in Situ</i> Diffuse Reflectance Spectroscopy. ACS Catalysis, 2019, 9, 6415-6424.	5.5	40
67	CO <sub>2</sub> capture, storage, and conversion using a praseodymium-modified Ga <sub>2</sub> O <sub>3</sub> photocatalyst. Journal of Materials Chemistry A, 2017, 5, 19351-19357.	5.2	38
68	Necessary and sufficient conditions for the successful three-phase photocatalytic reduction of CO <sub>2</sub> by H <sub>2</sub> O over heterogeneous photocatalysts. Physical Chemistry Chemical Physics, 2018, 20, 8423-8431.	1.3	38
69	Structural Analysis of Group V, VI, and VII Metal Compounds by XAFS. Journal of Physical Chemistry C, 2011, 115, 23653-23663.	1.5	36
70	Investigation of the electrochemical and photoelectrochemical properties of Ni–Al LDH photocatalysts. Physical Chemistry Chemical Physics, 2016, 18, 13811-13819.	1.3	36
71	Visible-Light Selective Photooxidation of Aromatic Hydrocarbons via Ligand-to-Metal Charge Transfer Transition on Nb <sub>2</sub> 0 <sub>5</sub> . Journal of Physical Chemistry C, 2017, 121, 22854-22861.	1.5	36
72	xTunes: A new XAS processing tool for detailed and on-the-fly analysis. Radiation Physics and Chemistry, 2020, 175, 108270.	1.4	36

#	Article	IF	CITATIONS
73	BrÃ,nsted Acid Generation over Alumina-Supported Niobia by Calcination at 1173ÂK. Catalysis Letters, 2009, 129, 383-386.	1.4	35
74	A unique photo-activation mechanism by "in situ doping―for photo-assisted selective NO reduction with ammonia over TiO2 and photooxidation of alcohols over Nb2O5. Catalysis Science and Technology, 2011, 1, 541.	2.1	35
75	Drastic improvement in the photocatalytic activity of Ga <sub>2</sub> O <sub>3</sub> modified with Mg–Al layered double hydroxide for the conversion of CO <sub>2</sub> in water. Sustainable Energy and Fuels, 2017, 1, 1740-1747.	2.5	35
76	Title is missing!. Topics in Catalysis, 2002, 18, 113-118.	1.3	34
77	Fabrication of well-shaped Sr2KTa5O15 nanorods with a tetragonal tungsten bronze structure by a flux method for artificial photosynthesis. Applied Catalysis B: Environmental, 2016, 199, 272-281.	10.8	34
78	Dual Ag/Co cocatalyst synergism for the highly effective photocatalytic conversion of CO <sub>2</sub> by H <sub>2</sub> O over Al-SrTiO <sub>3</sub> . Chemical Science, 2021, 12, 4940-4948.	3.7	34
79	Photoassisted NO reduction with NH3 over TiO2 photocatalyst. Chemical Communications, 2002, , 2742-2743.	2.2	33
80	XAFS and XRD Analysis of Ceria–Zirconia Oxygen Storage Promoters for Automotive Catalysts. Topics in Catalysis, 2008, 47, 137-147.	1.3	33
81	Visible-light-assisted selective catalytic reduction of NO with NH <sub>3</sub> on porphyrin derivative-modified TiO <sub>2</sub> photocatalysts. Catalysis Science and Technology, 2015, 5, 556-561.	2.1	33
82	Effect of Thickness of Chromium Hydroxide Layer on Ag Cocatalyst Surface for Highly Selective Photocatalytic Conversion of CO <sub>2</sub> by H <sub>2</sub> O. ACS Sustainable Chemistry and Engineering, 2019, 7, 2083-2090.	3.2	32
83	Modification of photocatalytic center for photo-epoxidation of propylene by rubidium ion addition to V2O5/SiO2. Catalysis Communications, 2005, 6, 269-273.	1.6	30
84	Ionic Liquid-Stabilized Single-Atom Rh Catalyst Against Leaching. CCS Chemistry, 2021, 3, 1814-1822.	4.6	30
85	Effect of Calcium Sulfate Addition on the Activity of the Absorbent for Dry Flue Gas Desulfurization. Energy & Fuels, 2001, 15, 438-443.	2.5	29
86	Role of lattice oxygen and oxygen vacancy sites in platinum group metal catalysts supported on Sr <sub>3</sub> Fe <sub>2</sub> O <sub>7â^î´</sub> for NO-selective reduction. Catalysis Science and Technology, 2018, 8, 147-153.	2.1	29
87	Isolated Platinum Atoms in Ni/γ-Al <sub>2</sub> O <sub>3</sub> for Selective Hydrogenation of CO <sub>2</sub> toward CH <sub>4</sub> . Journal of Physical Chemistry C, 2019, 123, 23446-23454.	1.5	29
88	Highly Active and Stable Pt–Sn/SBA-15 Catalyst Prepared by Direct Reduction for Ethylbenzene Dehydrogenation: Effects of Sn Addition. Industrial & Engineering Chemistry Research, 2017, 56, 7160-7172.	1.8	28
89	Size Controlled Synthesis of Gold Nanoparticles by Porphyrin with Four Sulfur Atoms. Topics in Catalysis, 2009, 52, 852-859.	1.3	27
90	Enhanced oxygen-release/storage properties of Pd-loaded Sr <sub>3</sub> Fe <sub>2</sub> O <sub>7â^îí</sub> . Physical Chemistry Chemical Physics, 2017, 19, 14107-14113.	1.3	27

#	Article	IF	CITATIONS
91	Valence Variation of Yb Encapsulated in the Supercage of Y-Type Zeolite. Japanese Journal of Applied Physics, 1993, 32, 481.	0.8	26
92	Oxygen Storage Property and Chemical Stability of SrFe <sub>1–<i>x</i></sub> Ti <sub><i>x</i></sub> O <sub>3â^î^</sub> with Robust Perovskite Structure. Journal of Physical Chemistry C, 2017, 121, 19358-19364.	1.5	26
93	Enhanced CO evolution for photocatalytic conversion of CO2 by H2O over Ca modified Ga2O3. Communications Chemistry, 2020, 3, .	2.0	26
94	Optimized Synthesis of Agâ€Modified Alâ€Doped SrTiO <sub>3</sub> Photocatalyst for the Conversion of CO <sub>2</sub> Using H <sub>2</sub> O as an Electron Donor. ChemistrySelect, 2020, 5, 8779-8786.	0.7	26
95	Highly Selective Photocatalytic Conversion of Carbon Dioxide by Water over Al-SrTiO <sub>3</sub> Photocatalyst Modified with Silver–Metal Dual Cocatalysts. ACS Sustainable Chemistry and Engineering, 2021, 9, 9327-9335.	3.2	26
96	Reaction Mechanism and the Role of Copper in the Photooxidation of Alcohol over Cu/Nb <sub>2</sub> O <sub>5</sub> . ChemPhysChem, 2011, 12, 2823-2830.	1.0	24
97	Flux method fabrication of potassium rare-earth tantalates for CO2 photoreduction using H2O as an electron donor. Catalysis Today, 2018, 300, 173-182.	2.2	24
98	Ni–Pt Alloy Nanoparticles with Isolated Pt Atoms and Their Cooperative Neighboring Ni Atoms for Selective Hydrogenation of CO <sub>2</sub> Toward CH <sub>4</sub> Evolution: <i>In Situ</i> and Transient Fourier Transform Infrared Studies. ACS Applied Nano Materials, 2020, 3, 9633-9644.	2.4	24
99	Selective reduction of NO over Cu/Al2O3: Enhanced catalytic activity by infinitesimal loading of Rh on Cu/Al2O3. Molecular Catalysis, 2017, 442, 74-82.	1.0	23
100	NOx Oxidation and Storage Properties of a Ruddlesden–Popper-Type Sr3Fe2O7â~'δ-Layered Perovskite Catalyst. ACS Applied Materials & Interfaces, 2019, 11, 26985-26993.	4.0	23
101	In Situ Time-Resolved Energy-Dispersive XAFS Study on Reduction Behavior of Pt Supported on TiO2 and Al2O3. Catalysis Letters, 2009, 131, 413-418.	1.4	22
102	Development of Rh-Doped Ga <sub>2</sub> O <sub>3</sub> Photocatalysts for Reduction of CO <sub>2</sub> by H <sub>2</sub> O as an Electron Donor at a More than 300 nm Wavelength. Journal of Physical Chemistry C, 2018, 122, 21132-21139.	1.5	22
103	Zeoliteâ€Encaged Pd–Mn Nanocatalysts for CO <sub>2</sub> Hydrogenation and Formic Acid Dehydrogenation. Angewandte Chemie, 2020, 132, 20358-20366.	1.6	22
104	Striking Oxygen-Release/Storage Properties of Fe-Site-Substituted Sr <sub>3</sub> Fe <sub>2</sub> O <sub>7â^`δ</sub> . Journal of Physical Chemistry C, 2018, 122, 11186-11193.	1.5	21
105	Structural analysis of tungsten–zirconium oxide catalyst by W Kâ€edge and L <sub>1</sub> â€edge XAFS. X-Ray Spectrometry, 2008, 37, 226-231.	0.9	19
106	X-Ray absorption spectroscopy (EXAFS/XANES) evidence for the preferential formation of isolated VO4 species on highly photoactive V2O5/SiO2 catalysts. Journal of the Chemical Society Chemical Communications, 1987, , 506.	2.0	18
107	Selective Catalytic Reduction of NO by NH <sub>3</sub> over Photocatalysts (Photo CR): Mechanistic Investigations and Developments. Chemical Record, 2016, 16, 2268-2277.	2.9	18
108	Metal oxide promoted TiO2 catalysts for photo-assisted selective catalytic reduction of NO with NH3. Research on Chemical Intermediates, 2008, 34, 487-494.	1.3	17

#	Article	IF	CITATIONS
109	Control of Acid-Site Location of MFI Zeolite by Catalytic Cracking of Silane and Its Application to Olefin Synthesis from Acetone. Journal of Chemical Engineering of Japan, 2009, 42, S162-S167.	0.3	16
110	Mechanism of NO–CO reaction over highly dispersed cuprous oxide on γ-alumina catalyst using a metal–support interfacial site in the presence of oxygen: similarities to and differences from biological systems. Catalysis Science and Technology, 2018, 8, 3833-3845.	2.1	16
111	Role of Bicarbonate lons in Aqueous Solution as a Carbon Source for Photocatalytic Conversion of CO <sub>2</sub> into CO. ACS Applied Energy Materials, 2019, 2, 5397-5405.	2.5	16
112	Self-regeneration of a Ni–Cu alloy catalyst during a three-way catalytic reaction. Physical Chemistry Chemical Physics, 2019, 21, 18816-18822.	1.3	16
113	Rational Design of a Molecular Nanocatalystâ€Stabilizer that Enhances both Catalytic Activity and Nanoparticle Stability. ChemCatChem, 2012, 4, 1907-1910.	1.8	15
114	Local Structure of Pr, Nd, and Sm Complex Oxides and Their X-ray Absorption Near Edge Structure Spectra. Journal of Physical Chemistry C, 2014, 118, 20881-20888.	1.5	15
115	Characterization of Cu Nanoparticles on TiO2 Photocatalysts Fabricated by Electroless Plating Method. Topics in Catalysis, 2014, 57, 975-983.	1.3	15
116	Recent progress in photocatalytic conversion of carbon dioxide over gallium oxide and its nanocomposites. Current Opinion in Chemical Engineering, 2018, 20, 114-121.	3.8	15
117	Fe-Modified CuNi Alloy Catalyst as a Nonprecious Metal Catalyst for Three-Way Catalysis. Industrial & Engineering Chemistry Research, 2020, 59, 19907-19917.	1.8	15
118	Imparting CO <sub>2</sub> reduction selectivity to ZnGa <sub>2</sub> O <sub>4</sub> photocatalysts by crystallization from hetero nano assembly of amorphous-like metal hydroxides. RSC Advances, 2020, 10, 8066-8073.	1.7	15
119	Generation of BrÃ,nsted Acid Over Alumina-Supported Niobia Calcined at High Temperatures. Topics in Catalysis, 2010, 53, 672-677.	1.3	14
120	Solvothermal Synthesis of Ca2Nb2O7 Fine Particles and Their High Activity for Photocatalytic Water Splitting into H2 and O2 under UV Light Irradiation. Chemistry Letters, 2015, 44, 1001-1003.	0.7	14
121	Local Structure and L1- and L3-Edge X-ray Absorption Near Edge Structure of Late Lanthanide Elements (Ho, Er, Yb) in Their Complex Oxides. Journal of Physical Chemistry C, 2015, 119, 8070-8077.	1.5	14
122	A detailed insight into the catalytic reduction of NO operated by Cr–Cu nanostructures embedded in a CeO <sub>2</sub> surface. Physical Chemistry Chemical Physics, 2018, 20, 25592-25601.	1.3	14
123	The importance of direct reduction in the synthesis of highly active Pt–Sn/SBA-15 for <i>n</i> -butane dehydrogenation. Catalysis Science and Technology, 2019, 9, 947-956.	2.1	14
124	Oxidation and Storage Mechanisms for Nitrogen Oxides on Variously Terminated (001) Surfaces of SrFeO <sub>3â^îſ</sub> and Sr <sub>3</sub> Fe <sub>2</sub> O <sub>7â^îſ</sub> Perovskites. ACS Applied Materials & Interfaces, 2021, 13, 7216-7226.	4.0	14
125	In situ observation of the dynamic behavior of Cu–Al–Ox catalysts for water gas shift reaction during daily start-up and shut-down (DSS)-like operation. Catalysis Science and Technology, 2012, 2, 1685.	2.1	13
126	Promoter effect of Pd species on Mn oxide catalysts supported on rare-earth-iron mixed oxide. Catalysis Science and Technology, 2016, 6, 7868-7874.	2.1	13

#	Article	IF	CITATIONS
127	Pd/SrFe <sub>1–<i>x</i></sub> Ti <sub><i>x</i></sub> O <sub>3â^Î</sub> as Environmental Catalyst: Purification of Automotive Exhaust Gases. ACS Applied Materials & Interfaces, 2018, 10, 22182-22189.	4.0	13
128	Deactivation Mechanism and Enhanced Durability of V <sub>2</sub> O <sub>5</sub> /TiO <sub>2</sub> –SiO <sub>2</sub> –MoO <sub>3</sub> Catalysts for NH <sub>3</sub> â^"SCR in the Presence of SO <sub>2</sub> . ChemCatChem, 2020, 12, 5938-5947.	1.8	13
129	Structural analysis of group V, VI, VII metal compounds by XAFS and DFT calculation. Journal of Physics: Conference Series, 2009, 190, 012073.	0.3	12
130	Photo-Induced Electron Transfer Between a Reactant Molecule and Semiconductor Photocatalyst: In Situ Doping. Catalysis Surveys From Asia, 2011, 15, 240-258.	1.0	12
131	Efficient oxygen storage property of Sr–Fe mixed oxide as automotive catalyst support. Journal of Materials Chemistry A, 2019, 7, 1013-1021.	5.2	12
132	Pt–Co Alloy Nanoparticles on a γâ€Al <sub>2</sub> O <sub>3</sub> Support: Synergistic Effect between Isolated Electronâ€Rich Pt and Co for Automotive Exhaust Purification. ChemPlusChem, 2019, 84, 447-456.	1.3	12
133	Dynamics of the Lattice Oxygen in a Ruddlesden–Popper-type Sr3Fe2O7â^'Î′ Catalyst during NO Oxidation. ACS Catalysis, 2020, 10, 2528-2537.	5.5	12
134	Metal Oxide Catalysts. Series on Synchrotron Radiation Techniques and Applications, 1996, , 304-325.	0.2	11
135	Photo-induced Surface Property on Transparent Mesoporous Silica Thin Films Containing Single-site Photocatalyst. Topics in Catalysis, 2008, 47, 116-121.	1.3	11
136	Sodium Cation Substitution in Sr <sub>2</sub> KTa <sub>5</sub> O <sub>15</sub> toward Enhancement of Photocatalytic Conversion of CO <sub>2</sub> Using H <sub>2</sub> O as an Electron Donor. ACS Omega, 2017, 2, 8187-8197.	1.6	11
137	Excellent Catalytic Activity of a Pdâ€Promoted MnO x Catalyst for Purifying Automotive Exhaust Gases. ChemCatChem, 2020, 12, 4276-4280.	1.8	11
138	Effect of molybdenum on the structure and performance of V2O5/TiO2–SiO2–MoO3 catalysts for the oxidative degradation of o-chlorotoluene. Applied Catalysis A: General, 2020, 595, 117496.	2.2	11
139	A feasibility study of "range-extended―EXAFS measurement at the Pt L <sub>3</sub> -edge of Pt/Al <sub>2</sub> O <sub>3</sub> in the presence of Au <sub>2</sub> O <sub>3</sub> . Journal of Analytical Atomic Spectrometry, 2018, 33, 84-89.	1.6	10
140	Low-temperature NO oxidation using lattice oxygen in Fe-site substituted SrFeO3â^î^. Physical Chemistry Chemical Physics, 2020, 22, 24181-24190.	1.3	10
141	Effect of Zn in Ag-Loaded Zn-Modified ZnTa <sub>2</sub> O <sub>6</sub> for Photocatalytic Conversion of CO <sub>2</sub> by H <sub>2</sub> O. Journal of Physical Chemistry C, 2021, 125, 1304-1312.	1.5	10
142	Efficient photocatalytic carbon monoxide production from ammonia and carbon dioxide by the aid of artificial photosynthesis. Chemical Science, 2017, 8, 5797-5801.	3.7	9
143	CO and C3H6 oxidation over platinum-group metal (PGM) catalysts supported on Mn-modified hexagonal YbFeO3. Catalysis Today, 2019, 332, 183-188.	2.2	9
144	Important Role of Strontium Atom on the Surface of Sr <sub>2</sub> KTa <sub>5</sub> O <sub>15</sub> with a Tetragonal Tungsten Bronze Structure to Improve Adsorption of CO <sub>2</sub> for Photocatalytic Conversion of CO <sub>2</sub> by H <sub>2</sub> O. ACS Applied Materials & Interfaces, 2019, 11, 37875-37884.	4.0	9

#	Article	IF	CITATIONS
145	Effect of Surface Reforming via O <sub>3</sub> Treatment on the Electrochemical CO <sub>2</sub> Reduction Activity of a Ag Cathode. ACS Applied Energy Materials, 2020, 3, 6552-6560.	2.5	9
146	Real-time observation of the effect of oxygen storage materials on Pd-based three-way catalysts under ideal automobile exhaust conditions: an <i>operando</i> study. Catalysis Science and Technology, 2021, 11, 6182-6190.	2.1	9
147	Strong Metal–Support Interaction in Pd/Ca2AlMnO5+δ: Catalytic NO Reduction over Mn-Doped CaO Shell. ACS Catalysis, 2021, 11, 7996-8003.	5.5	9
148	NO <sub><i>x</i></sub> Storage Performance at Low Temperature over Platinum Group Metal-Free SrTiO <sub>3</sub> -Based Material. ACS Applied Materials & Interfaces, 2021, 13, 29482-29490.	4.0	9
149	Shift of active sites via in-situ photodeposition of chromate achieving highly selective photocatalytic conversion of CO2 by H2O over ZnTa2O6. Applied Catalysis B: Environmental, 2021, 298, 120508.	10.8	9
150	Pore-Size Dependence of the Acidic Property of Mesoporous Silica FSM-16. Topics in Catalysis, 2009, 52, 657-663.	1.3	8
151	Photocatalytic Conversion of Carbon Dioxide over A <sub>2</sub> BTa <sub>5</sub> O <sub>15</sub> (A) Tj ETQ Engineering, 2018, 6, 8247-8255.	9q1 1 0.78 3.2	4314 rgBT ∣⊖ 8
152	Local Structure and L <sub>1</sub> - and L <sub>3</sub> -Edge X-ray Absorption Near Edge Structures of Middle Lanthanoid Elements (Eu, Gd, Tb, and Dy) in Their Complex Oxides. Inorganic Chemistry, 2021, 60, 9359-9367.	1.9	8
153	Effect of Cr Species on Photocatalytic Stability during the Conversion of CO <sub>2</sub> by H <sub>2</sub> O. Journal of Physical Chemistry C, 2019, 123, 2894-2899.	1.5	7
154	<i>In Situ</i> XANES Characterization of V <sub>2</sub> O <sub>5</sub> /TiO <sub>2</sub> –SiO <sub>2</sub> –MoO <sub>3</sub> Catalyst for Selective Catalytic Reduction of NO by NH <sub>3</sub> . Industrial & Engineering Chemistry Research, 2020, 59, 13467-13476.	1.8	7
155	Formation of CH <sub>4</sub> at the Metalâ€Support Interface of Pt/Al <sub>2</sub> O <sub>3</sub> During Hydrogenation of CO <sub>2</sub> : <i>Operando</i> XASâ€DRIFTS Study. ChemCatChem, 2022, 14, .	1.8	7
156	Oxygen Storage Capacity of Co-Doped SrTiO <sub>3</sub> with High Redox Performance. Journal of Physical Chemistry C, 2022, 126, 4415-4422.	1.5	7
157	Synthesis and Catalytic Performance of Organic–Inorganic Hybrid Mesoporous Material Having Basic Nanospace. Catalysis Letters, 2010, 140, 121-126.	1.4	6
158	Identification of hydrogen species on Pt/Al <sub>2</sub> O <sub>3</sub> by <i>in situ</i> inelastic neutron scattering and their reactivity with ethylene. Catalysis Science and Technology, 2021, 11, 116-123.	2.1	6
159	Recent Applications of X-ray Absorption Spectroscopy in Combination with High Energy Resolution Fluorescence Detection. Chemistry Letters, 2021, 50, 1075-1085.	0.7	6
160	Monolayer Tantalum Oxide on Mesoporous Silica Substrate. ChemistrySelect, 2016, 1, 3124-3131.	0.7	5
161	Quantum Chemical Computation-Driven Development of Cu-Shell–Ru-Core Nanoparticle Catalyst for NO Reduction Reaction. Journal of Physical Chemistry C, 2019, 123, 20251-20256.	1.5	5
162	Self-Regeneration Process of Ni–Cu Alloy Catalysts during a Three-Way Catalytic Reaction—An <i>Operando</i> Study. ACS Applied Materials & Interfaces, 2020, 12, 55994-56003.	4.0	5

#	Article	IF	CITATIONS
163	Photoelectrochemical investigation of the role of surface-modified Yb species in the photocatalytic conversion of CO2 by H2O over Ga2O3 photocatalysts. Catalysis Today, 2020, 352, 18-26.	2.2	5
164	Determination of Chemical States of Mercury on Activated Carbon Using XANES. AIP Conference Proceedings, 2007, , .	0.3	4
165	Active Center Induced by Vibronic Interactions in V2O5/SiO2. Topics in Catalysis, 2009, 52, 808-812.	1.3	4
166	Gold Nanoparticles Coated with Manganese–Porphyrin That Effectively Shorten the Longitudinal Relaxation Time of Water Molecules Depending on the Particle Size. Chemistry Letters, 2014, 43, 1901-1903.	0.7	4
167	Oxygen Release and Storage Property of Fe–Al Spinel Compounds: A Three-Way Catalytic Reaction over a Supported Rh Catalyst. ACS Applied Materials & Interfaces, 2021, 13, 24615-24623.	4.0	4
168	Development of Zinc Hydroxide as an Abundant and Universal Cocatalyst for the Selective Photocatalytic Conversion of CO 2 by H 2 O. ChemCatChem, 2021, 13, 4313.	1.8	4
169	Effect of Composition and Structure of Coating Polymers on Moisture Transporting Properties in Waterproof/Moisture-permeable Fabrics Prepared by Wet-Coagulation Process Seni Kikai Gakkai Shi/Journal of the Textile Machinery Society of Japan, 1996, 49, T49-T55.	0.0	4
170	XAFS Study of Active Tungsten Species on WO3/TiO2 as a Catalyst for Photo-SCR. AIP Conference Proceedings, 2007, , .	0.3	3
171	In situ time-resolved XAS study on metal-support-interaction-induced morphology change of PtO2 nanoparticles supported on γ-Al2O3 under H2 reduction. Catalysis Today, 2022, , .	2.2	3
172	Model building of metal oxide surfaces and vibronic coupling density as a reactivity index: Regioselectivity of CO2 adsorption on Ag-loaded Ga2O3. Chemical Physics Letters, 2019, 715, 239-243.	1.2	2
173	A theoretical investigation into the role of catalyst support and regioselectivity of molecular adsorption on a metal oxide surface: NO reduction on Cu/γ-alumina. Physical Chemistry Chemical Physics, 2021, 23, 2575-2585.	1.3	2
174	Observation of Adsorbed Hydrogen Species on Supported Metal Catalysts by Inelastic Neutron Scattering. Topics in Catalysis, 2021, 64, 660-671.	1.3	2
175	Frontiers of Photo-catalysis and Photo-reaction at Solid Surfaces. Photocatalysis by Silica Hyomen Kagaku, 1999, 20, 73-78.	0.0	1
176	Intermediate Valence State of La0.9Eu0.1Ni2(Si1-xGex)2Compounds. Journal of the Physical Society of Japan, 2003, 72, 2604-2607.	0.7	1
177	Energy-Dispersive XAFS Study on Reduction Behavior of Pt Supported on TiO2 and Al2O3. AlP Conference Proceedings, 2007, , .	0.3	1
178	Propane Metathesis by a Tandem Catalytic System: Dehydrogenation and Hydrogenation over PtSn/Al2O3, and Metathesis over Re2O7/Al2O3. Chemistry Letters, 2012, 41, 254-256.	0.7	1
179	Regioselectivity of H <sub>2</sub> Adsorption on Ga <sub>2</sub> O <sub>3</sub> Surface Based on Vibronic Coupling Density Analysis. Journal of Computer Chemistry Japan, 2018, 17, 138-141.	0.0	1
180	Probing the Entropic Effect in Molecular Noncovalent Interactions between Resinâ€Bound Polybrominated Arenes and Small Substrates. ChemPlusChem, 2018, 83, 820-824.	1.3	1

#	Article	IF	CITATIONS
181	Photocatalytic conversion of CO2 by H2O over heterogeneous photocatalysts. , 2020, , 179-190.		1
182	Effect of the in situ addition of chromate ions on H2 evolution during the photocatalytic conversion of CO2 using H2O as the electron donor. Catalysis Today, 2023, 410, 273-281.	2.2	1
183	Characterization of High Performance Materials by L-edge XANES in Soft X-ray Region Hyomen Kagaku, 1998, 19, 314-320.	0.0	Ο
184	Preparation of Ag-Loaded Ga <sub>2</sub> O <sub>3</sub> Particles by the Ultrasonic Reduction Method and their Photocatalytic Activities for CO <sub>2</sub> Reduction. Funtai Oyobi Fummatsu Yakin/Journal of the Japan Society of Powder and Powder Metallurgy, 2021, 68, 93-98.	0.1	0
185	Low-Temperature NOx Storage Capability of YBaCo4O7+Î′ Originating from Large Oxygen Nonstoichiometry. Industrial & Engineering Chemistry Research, 2021, 60, 9817-9823.	1.8	0
186	(Invited) Photocatalytic Conversion of CO2 By H2o As an Electron Donor over Ag/ZnGa2O4/Ga2O3. ECS Meeting Abstracts, 2015, , .	0.0	0
187	Dynamic behavior of Pd/Ca2AlMnO5+δ for purifying automotive exhaust gases under fluctuating oxygen concentration. Catalysis Today, 2022, , .	2.2	0